



I M A L

# IMAL preprints

ISSN 2451-7100

IMAL preprint #2023-0064

## FILTRATION EVOLUTION OF HYPERGRAPHS: A NOVEL APPROACH TO STUDYING MULTIDIMENSIONAL DATASETS

Dalma Bilbao - Hugo Aimar - Diego Mateos

 Publication Date: April 24, 2023

**Publisher:** Instituto de Matemática Aplicada del Litoral “Dra. Eleonor Harboure” (CONICET-UNL)



<https://imal.conicet.gov.ar>


<https://imal.conicet.gov.ar/preprints-del-imal>

**Publishing Director:** Dra. Estefanía Dalmaso



[edalmaso@santafe-conicet.gov.ar](mailto:edalmaso@santafe-conicet.gov.ar)

# Filtration Evolution of Hypergraphs: A Novel Approach to Studying Multidimensional Datasets

Dalma Bilbao<sup>1,3</sup>, Hugo Aimar<sup>1,3</sup>, and Diego M. Mateos <sup>1,2,3,\*</sup>

<sup>1</sup>Consejo Nacional de Investigaciones Científicas y Técnicas (CONICET), Argentina.

<sup>2</sup>Facultad de Ciencia y Tecnología. Universidad Autónoma de Entre Ríos (UADER). Oro Verde, Entre Ríos, Argentina.

<sup>3</sup>Instituto de Matemática Aplicada del Litoral (IMAL-CONICET-UNL), CCT CONICET, Santa Fé, Argentina.

\*Corresponding author: Diego M. Mateos, mateosdiego@gmail.com

## Abstract

The rapid growth of large datasets has led to a demand for novel approaches to extract valuable insights from intricate information. Graph theory provides a natural framework to model these relationships, but standard graphs may not capture the complex interdependence between components. Hypergraphs, are a powerful extension of graphs that can represent higher-order relationships in the data. In this paper, we propose a novel approach to studying the metric structure of a dataset using hypergraph theory and a filtration method. Our method involves building a set of hypergraphs based on a variable distance parameter, enabling us to infer qualitative and quantitative information about the data structure. We apply our method to various sets of points, dynamical systems, signal models, and real electrophysiological data. Our results show that the proposed method can effectively differentiate between different data sets, demonstrating its potential utility in a range of scientific applications.

**Keywords**— Hypergraphs, Metrics, Distances, Filtration

In this paper, we propose a novel approach to studying the metric structure of a data set using hypergraph theory and a filtration method. Our method involves building a set of hypergraphs based on a variable distance parameter  $r$ , enabling us to infer qualitative and quantitative information about the data structure. The choice of metric space used to define the distance between data points is based on the specific problem being addressed. To construct the hypergraphs, we define balls of radius  $r > 0$  centred at each data point and gradually increase the radius until the entire data set is covered, with the data falling into the balls forming the hyperedges. We employ a filtering method that enables us to study the relationships between the data as the radius changes, with different data topologies presenting different quantifier values that can distinguish between different systems. To evaluate our approach, we tested it on various sets of points, dynamical systems, signal models, and real electrophysiological data. Our results show that the method can effectively differentiate between these different data sets, demonstrating its potential utility in a range of scientific applications.

## 1 Introduction

Today, we have access to vast amounts of data, such as internet data, engineering signals, and medical images, unlike any other time in history. Extracting valuable information from these datasets using traditional statistical methods can be challenging. Furthermore, in most cases, it is essential to understand the relationship between the data components, which is often considered a pairwise relationship. Therefore, using graph theory is a natural approach to tackle this issue. However, in most real systems, the relationship between the data components is not bipartite. In such cases, the common practice is to compress these complex relationships between pairs, leading to a loss of valuable information. To overcome this problem, Berge introduced hypergraph theory [1, 2], which represents the multiple component relationships in a system. Hypergraph theory has been applied in various fields in recent years, such as signal analysis [3, 4], chemical reaction networks [5, 6], and biological networks [7, 8]. It has also been employed in the study of clinical pathologies, such as cardiac problems [9], neurodegenerative diseases [10], and epilepsy detection [11]. Additionally, hypergraphs have been widely utilized in the field of machine learning, including image classification [12], genetic algorithms [13], and the detection of COVID-19 in CT images. For a comprehensive review of hypergraph applications, refer to [14].

In this paper, we explore the application of hypergraph theory to analyze the metric structure of various types of data. To accomplish this, we use filtration techniques derived from algebraic topology. Rather than having a fixed hypergraph

for the data, we create a series of hypergraphs based on a variable parameter. This dynamic hypergraph approach provides a powerful tool for gaining qualitative and quantitative insights into the structure of the data.

Our approach is based on a finite set of data, which can take the form of points, signals, distributions, or images, among others. We define a notion of distance or similarity between the data points, which can be induced by the ambient space's metric (e.g., the Euclidean metric for data embedded in  $\mathbb{R}^n$ ) or defined by a pairwise distance matrix. The choice of metric is guided by the application.

We then define balls of radius  $r$  centered at each data point and incrementally increase the radius of these balls until they cover the entire dataset. The data points that fall within these balls form the hyperedges of the associated hypergraph. We generate hypergraphs for each radius and quantify the number of distinct hyperedges associated with each hypergraph. This filtering method allows us to study the relationships between the data that remain unchanged as the radius changes.

Different data topologies will exhibit different quantifier values, enabling us to distinguish between different systems. Overall, our approach provides a powerful tool for inferring robust qualitative and quantitative information about the data's structure.

In this scientific article, we present a study of various sets of points and data generated from different distributions and dynamical systems. The investigated data include two multidimensional systems: a Kuramoto model and magnetoencephalography data from an epilepsy patient. We employ different metric spaces to analyze the data and utilize a filtering method to generate the hypergraphs' dynamics. To quantify each hypergraph, we compute the number of hyperedges as a function of the radius  $r$ . Furthermore, we calculate the  $L^1$ -norm and Sobolev discrete seminorm  $\mathcal{S}$  for each generated curve, which allows us to collapse all the information into a single number.

Our results demonstrate that the proposed method can effectively differentiate all the analyzed data sets, including point distributions and dynamical systems. Specifically, we were able to quantify the transition between the uncoupled and fully coupled state of the Kuramoto model and detect changes in the signal dynamics of epileptic seizures. However, we acknowledge that the choice of metric space used to generate the distance matrix of each system may impact the obtained results. Nevertheless, this flexibility in selecting the underlying metric space enhances the method's robustness and flexibility, making it suitable for a wide range of applications.

Overall, our study highlights the potential of the proposed approach for analyzing complex data sets and gaining insights into their underlying structure. It provides a powerful tool for researchers across various domains to explore and interpret their data, paving the way for further advancements in data analysis and understanding complex systems.

## 2 Hypergraphs and covering

### 2.1 Hypergraphs

We shall follow the definition of hypergraph  $\mathcal{H}$  given by Berge in [1, 2]. Precisely, a hypergraph is a pair  $(\mathcal{V}, \mathcal{E})$ , where  $\mathcal{V}$  is the finite set of vertices and  $\mathcal{E}$  is a family of subsets of  $\mathcal{V}$  such that  $\mathcal{V} = \bigcup_{e \in \mathcal{E}} e$ . Each one of the elements  $e$  of  $\mathcal{E}$  is said to be a hyperedge. Notice that if the sets  $e \in \mathcal{E}$  have at most two elements  $\mathcal{V}$ , we have that  $\mathcal{H}$  is an undirected graph. Observe also that, being  $\mathcal{V}$  finite, we have that  $\mathcal{E}$  is also finite. An upper bound for the number of hyperedges is  $2^n - 1$ , where  $n$  is the number of elements of  $\mathcal{V}$ .

### 2.2 The general setting

Consider a set  $\chi$  that encompasses all potential data points, which can be deemed as a considerably large set. The elements in  $\chi$  can be associated with points in Euclidean space, denoted as  $\mathcal{R}^n$ , or even in functional space when the data points correspond to signals or images. In classical mathematical analysis such spaces can be taken to be Hilbert spaces, Banach spaces or even metric space. For the sake of generality, which allows us to consider non-symmetric "metrics" such as the Kullback-Leibler divergence, we shall not assume that  $\chi$  is a metric space. Instead, we shall start considering a more general metric-like structure, an  $\chi$ .

**Definition 1** A function  $\delta : \chi \times \chi \rightarrow \mathbb{R}_0^+$  shall called a "protometric" if  $\delta$  satisfies  $\delta(x, y) = 0$  if and only if  $x = y$ . The  $\delta$ -ball centered at  $x \in \chi$  with radius  $r > 0$  is defined by:  $\mathcal{B}_\delta(x, r) = \{ y \in \chi : \delta(x, y) < r \}$ .

Observe that with the above definition of protometric, in general  $\mathcal{B}_\delta(x, r)$  does not coincide with the set  $\{ y \in \chi : \delta(x, y) < r \}$  since  $\delta$  may not be symmetric. Of course every metric in  $\chi$  is a protometric. Recall that a metric  $d$  in  $\chi$  satisfies the additional properties:

- $d(x, y) = d(y, x)$  for every choice of  $x$  and  $y$  in  $\chi$ , and
- $d(x, z) \leq d(x, y) + d(y, z)$  for every choice of  $x, y$  and  $z$  in  $\chi$ .

Let  $\mathcal{V} = \{x_1, x_2, \dots, x_n\}$  be a finite sample of points in  $(\chi, d)$ . For any positive  $r$  and every  $i = 1, 2, \dots, n$ ; set

$$e_i(r) = \mathcal{B}_\delta(x_i, r) \cap \mathcal{V} = \{x_j \in \mathcal{V} : \delta(x_i, x_j) < r\},$$

and set  $\mathcal{E}(r)$  to denote the family  $\{e_i(r) : i = 1, \dots, n\}$  with radius  $r > 0$  fixed. Notice that the number of elements in  $\mathcal{E}(r)$  is some number  $\Delta^\mathcal{E}(r)$  between one and  $n$ . Since the  $e_i(r)$ 's clearly cover  $\mathcal{V}$ , we have the next statement.

**Proposition 1** For each  $r > 0$ , the couple  $(\mathcal{V}, \mathcal{E}(r))$  is a hypergraph with the additional property  $x_i \in e_i(r)$  for every  $i = 1, 2, \dots, n$ .

The idea is to consider this hypergraph structure as a function of  $r > 0$ . The next result contains some basic and elementary properties of this family of hypergraphs.

**Proposition 2** *Let  $(\mathcal{V}, \mathcal{E}(r))$  as before. Then*

- a)  $e_i(r_1) \subset e_i(r_2)$  if  $0 < r_1 \leq r_2 < \infty$ ;
- b)  $e_i(r) = \{x_i\}$  if  $0 < r \leq \min_j \delta(x_i, x_j)$ ;
- c)  $e_i(r) = \mathcal{V}$  if  $r > \max_j \delta(x_i, x_j)$ .

In other words, we have a family of hypergraphs starting at the trivial isolated points of  $\mathcal{V}$  and finishing at the trivial full hypergraph whose only hyperedge is  $\mathcal{V}$  itself.

Now we can generate an adjacency  $n \times n$  matrix  $\mathcal{A}(r)$  associated to the hypergraph  $(\mathcal{V}, \mathcal{E}(r))$  which is given by

$$\mathcal{A}(r) = \begin{pmatrix} 1 & \mathbb{I}_{e_2(r)}(x_1) & \dots & \mathbb{I}_{e_n(r)}(x_1) \\ \mathbb{I}_{e_1(r)}(x_2) & 1 & \dots & \mathbb{I}_{e_n(r)}(x_2) \\ \mathbb{I}_{e_1(r)}(x_3) & \mathbb{I}_{e_2(r)}(x_3) & \dots & \mathbb{I}_{e_n(r)}(x_3) \\ \vdots & \vdots & \ddots & \vdots \\ \mathbb{I}_{e_1(r)}(x_n) & \mathbb{I}_{e_2(r)}(x_n) & \dots & 1 \end{pmatrix} = (\mathbb{I}_{e_j(r)}(x_i))_{\substack{i=1,\dots,n \\ j=1,\dots,n}}$$

while  $\mathbb{I}_\theta$  is the indicator functional of  $\theta$ , i.e  $\mathbb{I}_\theta(x) = 1$  if  $x \in \theta$  and  $\mathbb{I}_\theta(x) = 0$  if  $x \notin \theta$ . Notice that if  $(\chi, d)$  is a metric space, then  $\mathcal{A}(r)$  is symmetric for every  $r > 0$ . In fact, since  $d(x, y) = d(y, x)$ , we readily have that  $\mathbb{I}_{e_j(r)}(x_i) = \mathbb{I}_{e_i(r)}(x_j)$ , because  $d(x_i, x_j) < r$  if and only if  $d(x_j, x_i) < r$ .

Notice also that for  $r > 0$  fixed it could happen that  $e_i(r) = e_j(r)$  for some  $i, j \in \{1, 2, \dots, n\}$ . In this case, the repeated column of the matrix (hyperedges) are eliminated, resulting in a new matrix  $\Delta^{\mathcal{E}}(r) \times n$  with  $\Delta^{\mathcal{E}}(r) \leq n$ . Let us call this matrix  $\mathbb{I}$  is, the incidence matrix of the hypergraph. Figure 1 shows an example of a hypergraph, and its associated incidence matrix.

### 2.3 Steps to build and characterize the hypergraphs $\mathcal{H}(r)$

Let us now proceed to summarize the algorithm used to analyze a set of data based on the characterization of hypergraphs. Given a data set,  $\mathcal{V} = \{x_1, \dots, x_n\}$  we generate and characterize the hypergraph associate to  $\mathcal{V}$  as follows:

---

#### Algorithm 1 Hypergraph filtration method

---

- 1: Define the distance  $d$  over the set  $\mathcal{V}$ .
- 2: Build the distance matrix  $\mathcal{D}_\chi = (d(x_i, x_j) : i, j = 1, \dots, n)$ .
- 3: For each,  $x_i \in \mathcal{V}$  define a ball centred in  $x_i$ :  $\mathcal{B}(x_i, r)$  with  $0 < r < 1$ .
- 4: Build the matrix  $\mathcal{M}$  for each  $r$  as

$$\mathcal{M}_{i,j}(r) = \begin{cases} 1 & \text{if } d(x_i, x_j) < r \\ 0 & \text{if } d(x_i, x_j) \geq r. \end{cases}$$

- 5: to obtain the  $\Delta^{\mathcal{E}}(r) \times n, \Delta^{\mathcal{E}}(r) \leq n$  incidence matrix,  $\mathcal{I}(r)$  eliminating the repeated columns of the matrix  $\mathcal{M}(r)$ .
  - 6: Compute the degree of hyperedges  $\Delta^{\mathcal{E}}(r)$ .
- 

### 2.4 Quantification of the curves $\Delta^{\mathcal{E}}(r)$

As we saw earlier, in the hypergraph filtering algorithm we see that the result is a function  $\Delta^{\mathcal{E}}(r)$ . From this curve, we can derive quantifiers which provide more compact information about the systems under investigation. In order to do this, we used  $L^1$ -norm ( $\mathcal{L}$ ) and the discrete Sobolev semi-norm of order 1 ( $\mathcal{S}$ ), which are explained below. Given a  $r$  running o to one, we discretize its value by taking  $r_i = i\Delta r$ ,  $i = 0, \dots, k-1$  and  $\Delta r = \frac{1}{k}$ .

The  $L^1$ -norm is given by

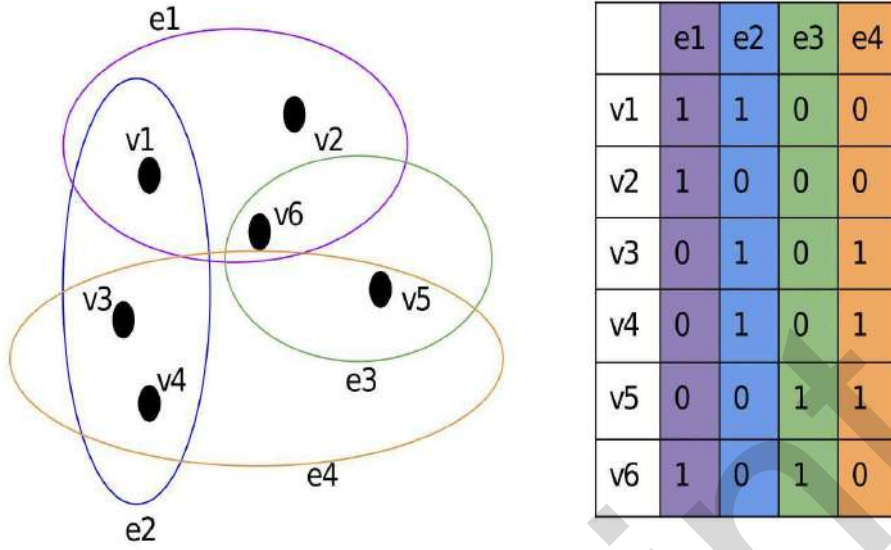
$$\mathcal{L} = \sum_{i=0}^{k-1} |\Delta^{\mathcal{E}}(r_i)|$$

and the Sobolev seminorm by

$$\mathcal{S} = \sum_{i=1}^{k-1} \frac{|\Delta^{\mathcal{E}}(r_i) - \Delta^{\mathcal{E}}(r_{i-1})|}{r_i - r_{i-1}}.$$

The underlying concept for utilizing these two metrics lies in their ability to measure and quantify the characteristics of the curves  $\Delta^{\mathcal{E}}$ . Specifically, the metric  $\mathcal{L}$  quantifies the area under the curve, while the metric  $\mathcal{S}$  measures the variations

A



B

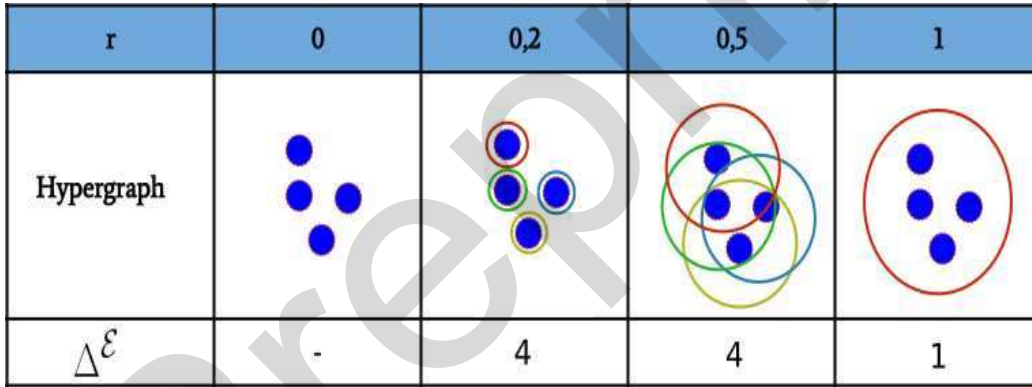


Figure 1: **A)** Example of incidence matrix for a hypergraph formed by 6 vertices and 4 hyperedges. **B)** Steps to build and measure the feature  $\Delta^{\mathcal{E}}(r)$  of the hypergraph for different values of  $r$ .

in the curve's slope. By incorporating these metrics, we can gain a more comprehensive understanding of the features and behavior exhibited by the curves  $\Delta^{\mathcal{E}}$ .

Additionally, it is often necessary to establish a notion of distance between systems, which can be achieved by measuring the distances between the curves  $\Delta^{\mathcal{E}}(r)$ . To accomplish this, we utilize the following pipeline:

We begin by considering two distinct sets of curves, namely  $\mathcal{V} = \Delta^{\mathcal{E}}(r)_1, \dots, \Delta^{\mathcal{E}}(r)_N$  and  $\hat{\mathcal{V}} = \Delta^{\mathcal{E}}(r)_1, \dots, \Delta^{\mathcal{E}}(r)_N$ , each comprising  $N$  realizations of a given system (e.g.,  $N$  different white noises). Next, we estimate the mean values  $\mu(r)$  and standard deviation  $\sigma(r)$  for each group. Finally, we calculate the distance between the two groups, denoted as  $d^{\mathcal{V}, \hat{\mathcal{V}}}(r)$ , using the following method.

If  $\sigma(r) < \hat{\sigma}(r)$  then

$$d^{\mathcal{V}, \hat{\mathcal{V}}}(r) = \begin{cases} (\mu(r) - \sigma(r)) - (\hat{\mu}(r) + \hat{\sigma}(r)) & \text{if } (\mu(r) - \sigma(r)) > (\hat{\mu}(r) + \hat{\sigma}(r)) \\ 0 & \text{if } (\mu(r) - \sigma(r)) \leq (\hat{\mu}(r) + \hat{\sigma}(r)) \end{cases}$$

or  $\sigma(r) > \hat{\sigma}(r)$  then

$$d^{\mathcal{V}, \hat{\mathcal{V}}}(r) = \begin{cases} (\hat{\mu}(r) - \hat{\sigma}(r)) - (\mu(r) + \sigma(r)) & \text{if } (\hat{\mu}(r) + \hat{\sigma}(r)) > (\mu(r) - \sigma(r)) \\ 0 & \text{if } (\hat{\mu}(r) - \hat{\sigma}(r)) \leq (\mu(r) + \sigma(r)) \end{cases}$$

Finally we quantify the difference applying the two norms described before  $L^1$ -norm and Sovolev semi-norm of order 1 to

the distance vector  $d^{\mathcal{V}, \hat{\mathcal{V}}}(r)$ .

### 3 Results

This work utilizes the metric hypergraph filtering method to analysed four distinct databases, comprising three artificial and one real dataset. The first dataset involves the characterization and differentiation of five sets of points in  $\mathbb{R}^3$  exhibiting unique probability distributions. In the second example, the similarities and differences among three dynamical systems and one stochastic system in  $\mathbb{R}^3$  were analyzed. The third example focuses on the dynamics of a system of coupled oscillators, utilizing the Kuramoto model. Lastly, the dynamics of magnetoencephalography (MEG) recordings from two patients experiencing generalized epilepsy during an epileptic seizure were examined.

#### 3.1 Point distribution

The first example to study were a set of points in  $\mathbb{R}^3$  generated under different distributions: i) Normal, ii) Uniform, iii) Poisson, and generated with a specific structure iv) Lattice and v) Fractal (see Figure 2A). Additional information regarding these distributions is available in the appendix B.

For each set, we generated 100 realizations of 1000 points each. To obtain the incidence matrix, we employed the filtering method outlined in section 2.4, utilizing different distances  $\mathcal{D}$ . The following metrics were employed to calculate the distances between points: i) Chebyshev, ii) Cityblock, iii) Euclidean, iv) Minkowski, and v) Parabolic (with  $\alpha^1 = 1$ ,  $\alpha^2 = 1/2$ ,  $\alpha^3 = 1/2$ ) -additional information on these metrics can be found in A. Using  $\mathcal{L}$  and  $\mathcal{S}$  distances introduced in section 2.4, we characterized the  $\Delta^\mathcal{E}(r)$  curves. Finally, employing the pipeline described in 2.4, we calculated the distances between the systems.

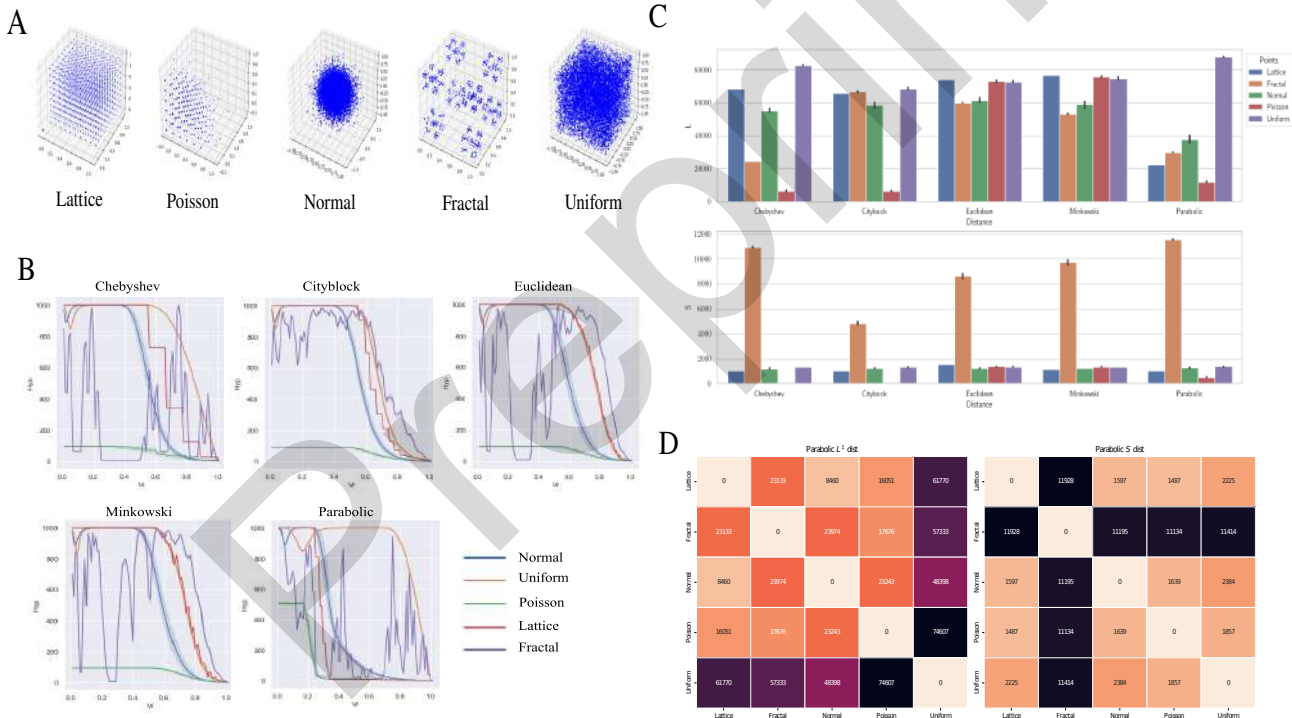


Figure 2: **A)** Examples of different points distribution used in the analysis. **B)** Analysis of the number of hyperedges versus parameter  $r$ , for  $\mathbb{R}^3$  data points distribution. Each subplot represents the distance metric used to obtain the hypergraph. **C)** Values of  $L^1$ -norm  $\mathcal{L}$  and Sobolev seminorm  $\mathcal{S}$  for the different distributions points and metric spaces used. **D)** Distance matrix  $\mathcal{L}$  and  $\mathcal{S}$  between the different point distributions analysed on the metric parabolic space.

The analysis of the number of hyperedges  $\Delta^\mathcal{E}$  for each distance metric enables clear differentiation among the five types of point distribution, with the Chebyshev and Parabolic distances exhibiting particularly notable distinctions. Notably, the isotropic metrics ( $\mathcal{D}^{Euc}$ ,  $\mathcal{D}^{Cheb}$ ,  $\mathcal{D}^{City}$ ,  $\mathcal{D}^{Mink}$ ) display a lattice array beginning with a number of hyperedges similar to that of vertices, which remains constant until  $r$  approaches  $r = 0.58$ . Subsequently, the number of hyperedges decreases until reaching zero, though this decrease is non-uniform and fluctuating for the Euclidean and Minkowski distances and stepwise for the Chebyshev and Cityblock distances. In contrast, the behaviour of the Parabolic distance is distinct, with the number of hyperedges starting very low, approximately  $\Delta^\mathcal{E} \sim 150$ , and dropping to zero at  $r \sim 0.28$ .

Regarding the Normal distribution, it is observed that the number of hyperedges is comparable to the number of vertices for small values of  $r$ . At approximately  $r \sim 0.06$ , a drop in  $\Delta^\mathcal{E}$  is apparent, though it rapidly returns to its initial

values. Ultimately, a uniform reduction in the number of hyperedges is observed, leading to a complete reduction to zero for  $r = 1$ . This behaviour occurred at approximately  $r \sim 0.6$  for the isotropic distances, while it occurs at roughly  $r \sim 0.3$  for the parabolic distance.

The uniform distribution exhibits a similar pattern to the Normal distribution, but the decrease in the number of hyperedges is uniform and begins earlier, before  $r \sim 0.6$ , for all metrics. The Poisson distribution demonstrates a high degree of data clustering, resulting in a lower number of hyperedges even for small values of  $r$ . These values remain constant until  $r \sim 0.06$ , at which point they uniformly decrease to zero across all metrics. The fractal distribution displays a distinctive behaviour compared to the other distributions. The number of hyperedges strongly depends on the  $r$  values, and the curves demonstrate periodic fluctuations, particularly for the Chebyshev and Parabolic distances. These fluctuations include intervals of low numbers of hyperedges that alternate with peaks of high  $\Delta^\epsilon$  values. Similar behaviour is seen for the other metrics within the range of  $0 < r \leq 0.7$ , after which  $\Delta^\epsilon$  decays uniformly to zero beyond  $r \sim 0.7$ .

In Figure 2C, we present the measurements of  $\mathcal{L}$  (top) and  $\mathcal{S}$  (bottom) for all the point distributions and metrics. Our observations indicate that the Chebyshev and Parabolic distances provide the best discriminators between the point distributions in terms of  $\mathcal{L}$ . The uniform distribution has the highest  $\mathcal{L}$  value, while the Poisson distribution has the lowest. Moreover, the relative values between the distributions show significant variations depending on the chosen metric. In the case of  $\mathcal{S}$  values, we observe that the fractal arrangement has substantially higher values compared to the other distributions. However, no significant differences are observed between the other distributions for all the distances used.

Finally, Figure 2D displays the distance matrices  $\mathcal{L}$  and  $\mathcal{S}$  for the different point distributions in the parabolic metric space. Notably, all distances in both matrices are non-zero, indicating that according to the significance definition proposed in Section 2.4, all distributions exhibit marked differences from each other in the parabolic metric space.

### 3.2 Dynamical Systems

The second type of data set comprises 3-dimensional chaotic systems: i) Rossler map, ii) complex butterfly map, iii) Lorenz map, and iv) white noise (see Figure 3A). To generate each system's data, we created 100 sequences, each consisting of 10000 data points, and then subsampled them to 1000 data points. More detailed information about the data sets generated can be found in Appendix B.

Figure 3B presents the analysis of the number of hyperedges  $\Delta^\epsilon$  as a function of the parameter  $r$ , showing the ability of different distance metrics to differentiate the four chaotic systems: Rossler map, complex butterfly map, Lorenz map, and white noise. The results indicate that the Chebyshev and Parabolic distance (with  $\alpha^1 = 1, \alpha^2 = 1/2, \alpha^3 = 1/2$ ) are the most effective at distinguishing between the systems, while the Euclidean distance fails to do so.

For white noise, all metrics show a similar number of hyperedges and vertices for small values of  $r$ , with a decrease around  $r \sim 0.06$ , followed by a rapid return to the original values, and then higher values of  $\Delta^\epsilon$  until  $r \sim 0.5$  for isotropic metrics and  $r \sim 0.3$  for parabolic distances, before uniformly decreasing to zero at  $r = 1$ .

The Rossler map starts with  $\Delta^\epsilon < N_{vert}$  for isotropic metrics but rapidly rises near the maximum at  $r \sim 0.2$  and remains high until  $r \sim 0.6$ , before decaying to zero. However, for the parabolic distance (a non-isotropic measure), the curve's behaviour is different, decreasing sharply at  $r \sim 0.15$  and changing the slope at  $r \sim 0.2$ .

The complex butterfly and Lorenz maps show similar behaviour for isotropic metrics, except for Chebyshev, where the slope changes slightly between them. However, for the parabolic distance, the differences between these two chaotic maps are remarkable. Similarly, for the Lorenz map, only the parabolic distance can clearly distinguish it from the other dynamical systems.

In Figure 3C, we can see the values of  $\mathcal{L}^1$  (top) and  $\mathcal{S}$  (bottom) for all the dynamical and stochastic systems and metrics used. The results show that Cityblock distance is the best discriminator between points for  $\mathcal{L}$ . For all metrics, Complex Butterfly shows a significant difference from the other systems. The Euclidean, Minkowski, and parabolic metrics cannot distinguish between Lorenz map, Rossler map, and white noise. In the case of  $\mathcal{S}$ , the only metric space that allows clear identification between the systems is the parabolic one; in other spaces, there is no clear difference between the systems.

To better understand the results, we looked at Figure 3C and found that the Chebyshev distance for  $\mathcal{L}$  and the Parabolic distance for  $\mathcal{S}$  are the best metrics to measure the distance between the systems. The corresponding distance matrices are shown in Figure 3D. We observed that all systems have significantly different distances in the  $\mathcal{L}$  matrix, with the Complex Butterfly having the largest distance compared to the other systems. In the  $\mathcal{S}$  matrix, the largest distances are between the dynamical systems and white noise.

### 3.3 Kuramoto Model

The third example to which we apply hypergraph filtering is to study the dynamics of the Kuramoto model for 100 oscillators.

The Kuramoto model is a mathematical model used to describe the collective behaviour of a group of coupled oscillators [15]. In this model, each oscillator is characterized by its phase, which evolves according to its intrinsic frequency as well as the strength of the coupling to other oscillators in the system.

The model is often used to describe synchronization phenomena in nature, such as the synchronization of fireflies flashing in unison. The Kuramoto model has been applied to a variety of systems, including neural networks, power grids, and opinion dynamics [16, 17].

The Kuramoto model is a mathematical description of synchronization in networks of coupled dynamical systems [15], which has been widely used in neuroscience to study the collective behaviour of coupled neuronal oscillators [17, 18]. It is

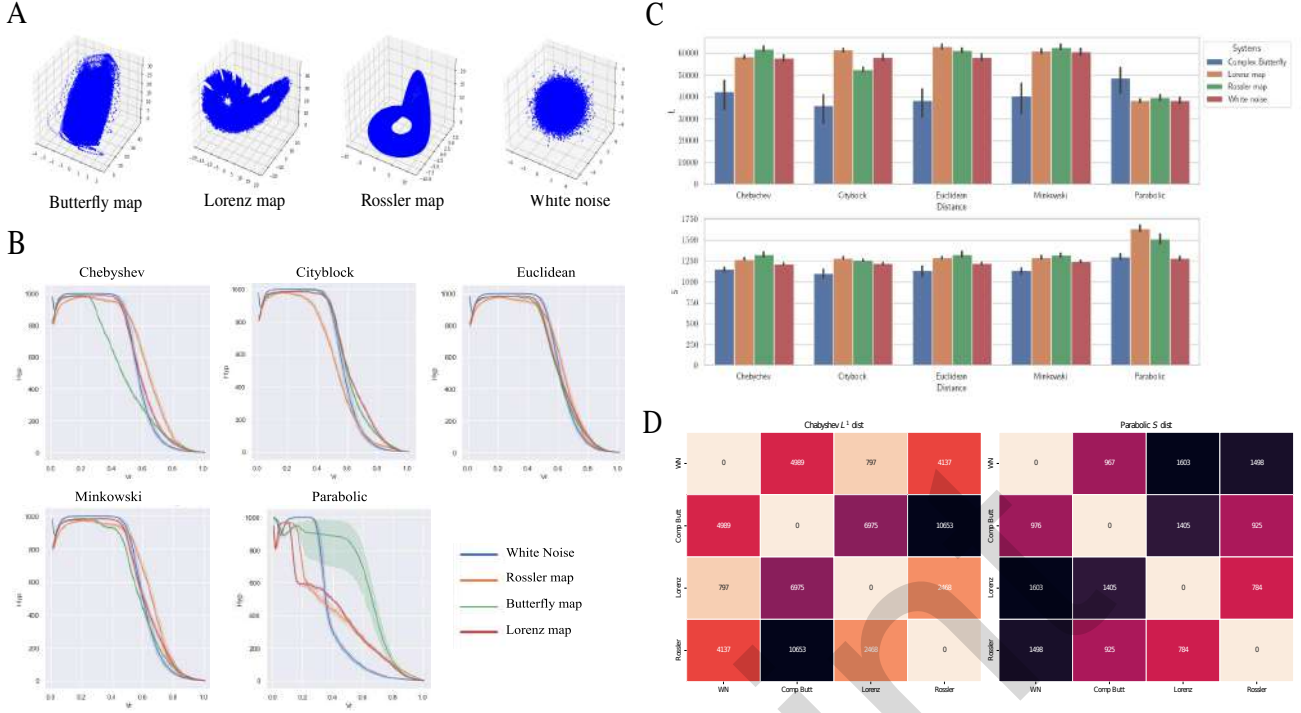


Figure 3: **A)** Examples of the three dynamical system and the stochastic system used in the analysis **B)** Analysis of the number of hyperedges versus parameter  $r$ , for three dynamical system and white noise. Each subplot represents the distance metric used to obtain the hypergraph. **C)** Values of  $L^1$ -norm  $\mathcal{L}$  and Sobolev seminorm  $\mathcal{S}$  for the different distributions points and metric spaces used. **D)** Distance matrix  $\mathcal{L}$  and  $\mathcal{S}$  between the different dynamical system analysed

based on the concept of phase synchronization, whereby the phases of neighbouring oscillators become increasingly aligned over time. The model has been used to explain a variety of phenomena in the brain, including synchronization of neurons in the hippocampus, the emergence of gamma oscillations in the visual cortex, and the generation of rhythms in the basal ganglia. The model proposes that neurons form clusters of synchronous activity, and this can lead to the generation of seizures. In the most widely used version of the Kuramoto model, each of the oscillators is considered to have its own eigenfrequency  $\omega_i$ , and each is equally coupled to all other oscillators. The Kuramoto model equation is given by:

$$\frac{d\theta_i}{dt} = \omega_i + \frac{K}{N} \sum_j \sin(\theta_j - \theta_i) \quad i = 1 \dots N$$

Where  $\theta_i$  is the phase of the  $i$ -th oscillator,  $\omega_i$  is the natural frequency of the  $i$ -th oscillator,  $K$  is the coupling strength between the oscillators, and  $N$  is the number of oscillators.

In this work, we use  $N = 100$  oscillators with a coupling constant of  $K = 2.8$ . The initial network condition was based on the Erdős-Renyi model for a probability of  $P = 1$ . The system was allowed to evolve for a period of,  $T = 10$  with a step of  $dt = 0.1$ . Figure 4A shows the time series  $\sin\theta(t)$ . For each time,  $t$  the distance matrix  $\Delta_{i,j}$  between all pairs of oscillators  $i, j$ ,  $i \neq j$  was calculated. To this matrix, we applied the method developed in 2.3 to obtain the values of the number of hyperedges as a function of  $r$  and time  $\Delta^{\mathcal{E}}(r, t)$  (see 4 B). Finally, we compute the norm  $\mathcal{L}(t)$  and  $\mathcal{S}(t)$  as a function of time (see 4 C, D).

As we explained before, as time evolves, the system undergoes a transition from an uncoupled state to a fully coupled state. This transition is reflected in the  $\Delta^{\mathcal{E}}(r, t)$  curves, where the number of hyperedges decay more rapidly to zero as the system couples, ultimately reaching a point where the number of hyperedges is  $\Delta^{\mathcal{E}}(r, t = 10) = 1$  for all  $r$  (in the case of full coupling). This behaviour is clearly quantified using  $\mathcal{L}$  and  $\mathcal{S}$  metrics, as shown in Figures 4C, D, where both distances decrease as the system couples.

### 3.4 Seizure detection

In this section, we will give an example of the application of the hypergraph filtering method to the analysis of multi-dimensional electrophysiological signals. In particular, we will study the dynamics of a magnetoencephalography (MEG) signals belonging to two patients with generalized epilepsy.

Seizure dynamics involve abnormal and excessive electrical activity in the brain that can lead to a variety of physical and cognitive symptoms. In order to understand and treat seizure dynamics, it is important to understand how the brain's electrical activity changes during a seizure. This includes studying how different brain regions interact with each other,



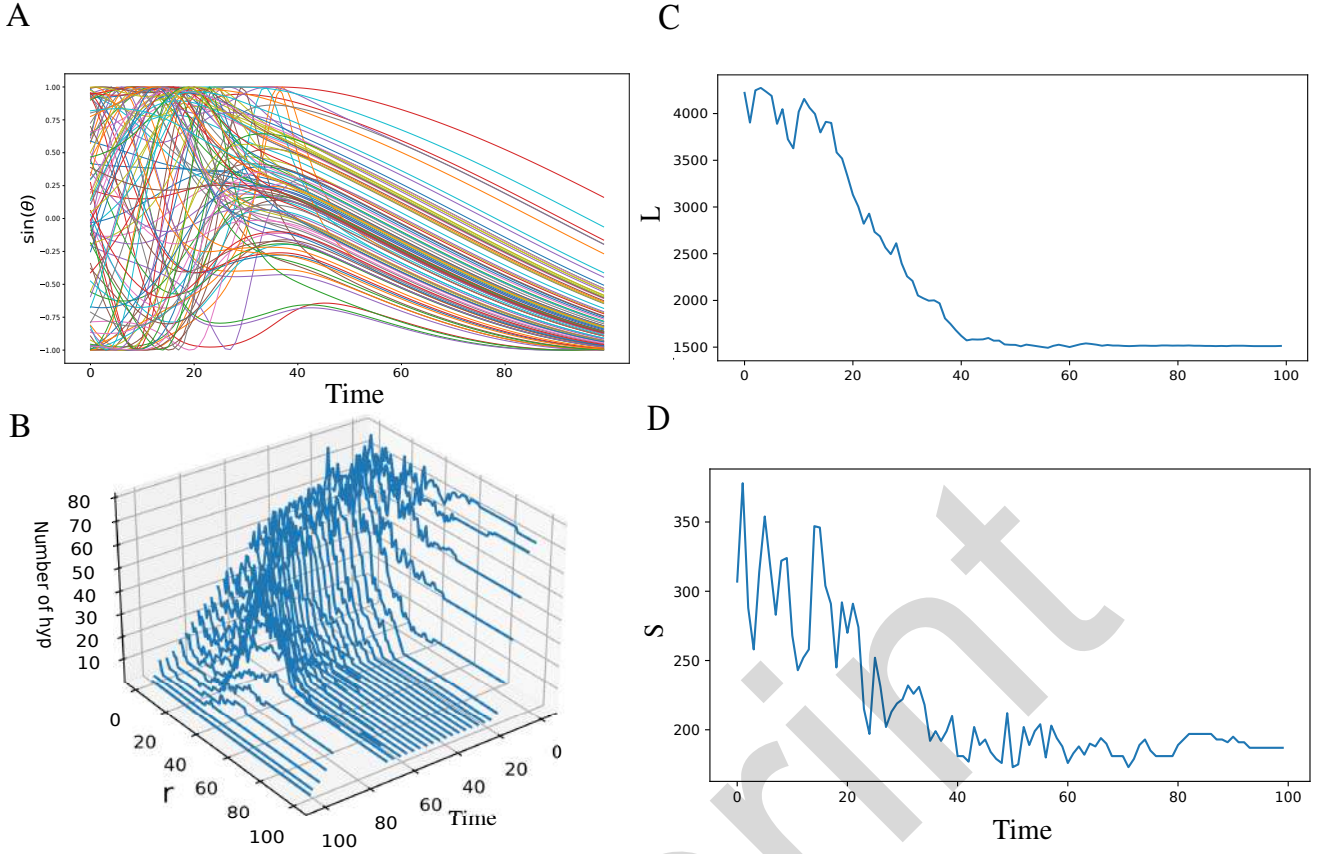


Figure 4: **A)** Time series for the  $N = 100$  oscillator. **B)** Number of hyperedges  $\Delta^{\mathcal{E}}(r, t)$  in function of  $r$  and time. **C)**  $L^1$ -Norm ( $\mathcal{L}$ ) over the time **D)** Sovolev seminorm  $\mathcal{S}$  over the time

how the electrical activity of neurons changes, and how the seizure progresses over time. Because of this, the study of the relationship between electrophysiological signals is of paramount importance for understanding the coupled dynamics occurring at seizure onset.

We analysed two patients suffering for epilepsy. The former had primary generalized epilepsy and the latter had secondary generalized epilepsy. Details of the patients' epilepsy, seizure types and specifications can be found in previous work [19]. Each patient was recorded by magnetoencephalography (MEG) in basal and ictal (seizure) periods. Recording was performed using a 144-channel MEG with a sampling rate of 625 Hz. An example of a MEG channel recording is shown in Figure 5A. For the analysis, we used the 144 MEG signals embedded in a metric space that calculates the distance between signals based on their phase difference. The method used to measure these distances (or connectivity) was the *Phase Locking Index* (PLI) [20]. To do this, the raw recording was cut into segments of 5s epochs, overlapping at %50. For each segment, we calculated the distance matrix of  $144 \times 144$ . In total, we obtain  $N = 46$  connectivity matrices. For every matrix, we applied the hypergraph filtering method described above, to compute  $\Delta^{\mathcal{E}}(r, t)$  and the corresponding  $\mathcal{S}(t)$  and  $\mathcal{L}(t)$ .

The results indicate that both patients showed similar behaviour in the basal state (blue lines in Figure 5B), with high values of the number of hyperedges  $\Delta^{\mathcal{E}bl}(r, t)$  that remained constant until  $r = 0.8$ , where it suddenly dropped to  $\Delta^{\mathcal{E}bl}(r = 1) = 1$ . During the seizure attack (red line), the topology of  $\Delta(r)_{sz}$  changed significantly, with high values at the start, but a quicker decrease at  $r = 0.2$  for patient 1 and  $r = 0.4$  for patient 2. After the attack, in the post-ictal period (blue lines), the values of  $\Delta^{\mathcal{E}pi}(r, t)$  returned to their baseline-like behaviour.

These dynamics can be quantified more concisely by calculating  $\mathcal{L}$  and  $\mathcal{S}$  (shown in Figure 5C, D). Looking at the  $\mathcal{L}$  values over time, we see that they remained constant for both patients until the seizure attack (SZ period), where they abruptly dropped and then returned to their original values in the post-ictal state. This behaviour is due to the changes in the shape of the  $\Delta^{\mathcal{E}bl}(r, t)$  curves during the attack. The  $\Delta_{sz}^{\mathcal{E}}(r, t)$  curves decayed faster to zero, with a smaller area compared to the base or post-ictal state ( $\Delta_{bl/pi}^{\mathcal{E}}(r, t)$ ). On the other hand, the  $\mathcal{S}$  analysis detected the attack for patient 1, showing an increase in the SZ values, but it did not detect the attack for patient 2. This result indicates that the seizure dynamics for both patients were different.

## 4 Discussion

In this work, we introduce a novel approach to study different multidimensional datasets from point distribution, dynamical systems and electrophysiological signals, using a method of filtration evolution of the hypergraph. The method introduce

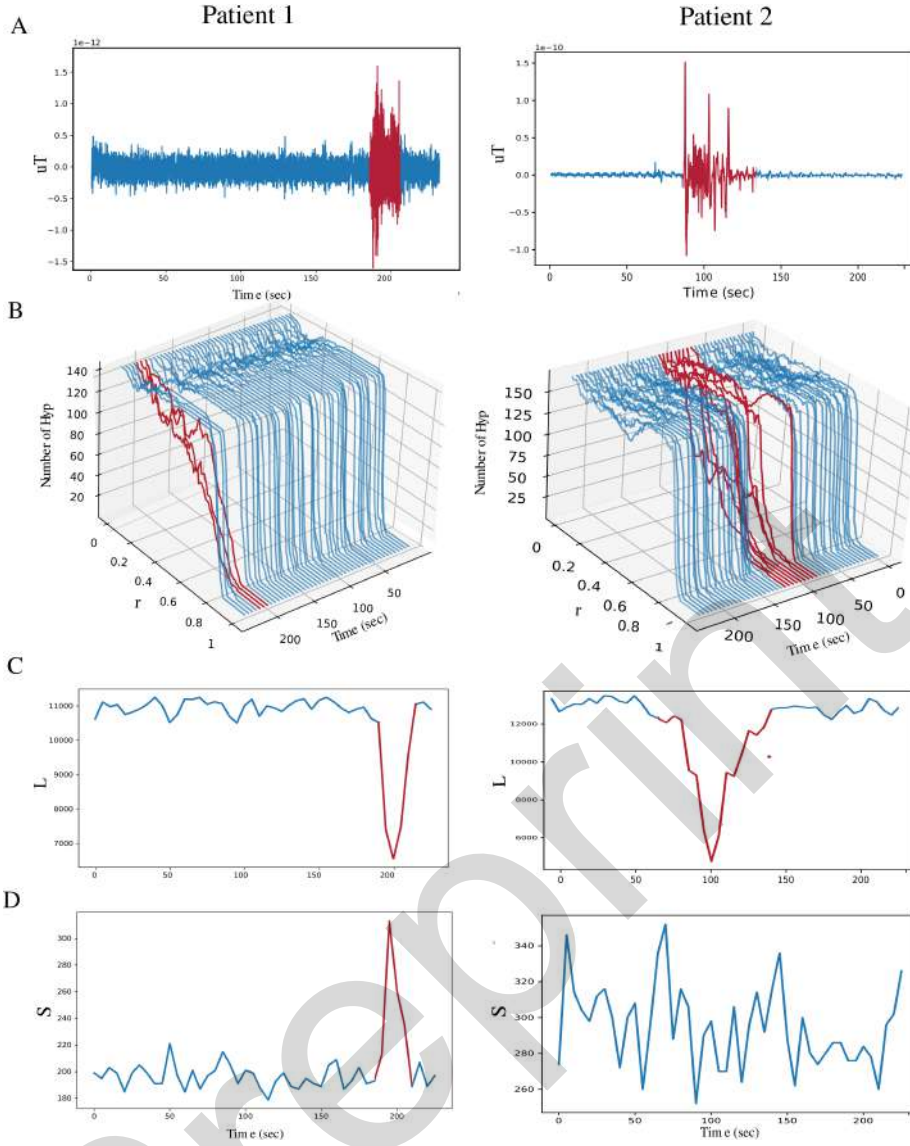


Figure 5: Filtration Hypergraph method applied over two magnetoencephalography signals belong to two patient with generalize epilepsy (patient 1 left row and patient 2 right row) **A)** Example of one channel of MEG signal, **B)** Number of hyperedges over  $r$  and time ( $\Delta^e(r, t)$ ). The blue lines represent the baseline and postictal states, the red one are the seizures periods. **C)**  $L^1$  norm versus time analysis. **D)** Sobolev seminorm  $S$  versus time analysis.

in this paper shows the strength to extract information about the structure and relation of the component of the dataset.

The behaviour of  $\Delta^e(r)$  is strongly influenced by the underlying metric space in which the data is embedded. Different metric spaces can give rise to distinct patterns of clustering and sparsity, resulting in varying values of  $\Delta^e(r)$  for a given radius  $r$ . For example, in Euclidean space, points are defined by their distance from one another, and  $\Delta^e(r)$  tends to decrease as  $r$  it increases, reflecting a transition from a sparser distribution of points to a more clustered one. Understanding the behaviour of  $\Delta^e(r)$  in different metric spaces is crucial for correctly interpreting and analysing data, as it can reveal key insights into the underlying structure and organization of the data.

A high value of  $\Delta^e(r)$  is indicative of low data clustering, which is observed when the radius  $r$  is small and the number of adjacent points is minimal. For instance, in the case of point distributions or dynamical systems with  $r \sim 0$ , the number of hyper-artists is similar to the number of points, leading to a  $\Delta^e(r)$  value approximately equal to  $N$ . Exceptions to the low clustering behaviour can arise in certain scenarios, such as the Poisson point distribution, where points are densely packed together such that even with a small radius, neighbouring points fall within the same ball. This high-density phenomenon can lead to a strong compression of points, and thus higher clustering, despite the small radius.

In datasets with isotropic topology, the choice of metric does not significantly impact the characterization of the data. However, for datasets with non-isotropic topology, such as those generated by the Lorenz or Rossler maps, standard isotropic metrics like Euclidean distance and Chebyshev distance may not be suitable for accurately characterizing the data. Instead, non-isotropic metrics like the parametric metric can provide a better differentiation between the systems in

question. Thus, the choice of metric must be carefully considered, ensuring an accurate characterization of the underlying structure and organization of the data.

The  $L^1$ -Norm ( $\mathcal{L}$ ) and Sobolev seminorm ( $\mathcal{S}$ ) are valuable metrics for quantifying the curves  $\Delta^\varepsilon(r)$  obtained through the filtration method. These metrics help to provide a comprehensive understanding of the curves' properties. Additionally, the proposed pipeline for measuring the distance between two curves allows for the identification of differences that may not be apparent by comparing only their intrinsic values, such as  $\mathcal{L}$  and  $\mathcal{S}$ . By incorporating this pipeline, a more complete and nuanced analysis of the curves can be obtained.

The filtration hypergraph pipeline also shows the effectiveness of different distance metrics in quantifying the properties of various chaotic and stochastic systems. For these cases, the Chebyshev and Parabolic distances were found to be the most effective in differentiating the four dynamical systems studied, while the Euclidean distance was not able to distinguish between them. Moreover, using  $\mathcal{L}^1$  and Sobolev seminorm  $\mathcal{S}$  metrics were also found to be effective discriminators, with the Cityblock distance being the best for  $\mathcal{L}^1$  and the Parabolic distance being the best for  $\mathcal{S}$ . These findings are significant because they demonstrate the capacity of characterizing complex systems.

For the case of different point distributions and distance metrics, the results show that the Chebyshev and Parabolic distances are more effective in distinguishing between different point distributions. The Poisson distribution shows a higher data clusterization with a lower number of hyperedges, while the Fractal distribution shows a different behaviour with fluctuations and alternating periods of low and high numbers of hyperedges. The Chebyshev and Parabolic distance metrics are the best discriminators between points for  $\mathcal{L}$ , with the highest values corresponding to the uniform distribution and the lowest to the Poisson distribution. The fractal arrangement has significantly higher values than the other distributions for  $\mathcal{S}$ . The results emphasize the importance of selecting appropriate distance metrics when analysing point distributions, as the relative values between distributions can vary significantly depending on the metric used.

This method has an important feature of enabling the examination of the time evolution of various types of dynamical systems, as demonstrated by the study of the Kuramoto coupled model. The analysis allowed the characterization of the transition from a completely uncoupled to a fully coupled system, using the  $\Delta^\varepsilon$  curves and  $\mathcal{L}$  and  $\mathcal{S}$  metrics. These results offer a powerful tool for comprehending the system's dynamics and transitions. The study's findings are significant as they provide a quantitative understanding of the synchronization behaviour in the Kuramoto model, which has broad applications across multiple scientific disciplines, including physics, engineering, and neuroscience.

For the study of the dynamical evolution of the MEG signals in epileptic patients, we can see there are significant changes in the brain's network topology during the onset and post-ictal periods of seizures. The number of hyperedges in the brain network behaves similarly in the basal state for both patients, but changes markedly during the seizure period, with a faster decay in hyperedge values in the second patient. The  $\mathcal{L}$  values of the network show a drop during the seizure period and a return to baseline values in the post-ictal state for both patients. However, the  $\mathcal{S}$  analysis shows that the seizure was detected in patient 1 but not in patient 2, indicating that the dynamics of the seizure are different between the two patients. These findings suggest that analysing brain network topology may be a useful tool for studying seizure dynamics and may help in developing new approaches for seizure detection and treatment.

Finally, in this study, we have used the number of hyperedges as a metric or feature to quantify the hypergraph evolution. However, it is important to note that there may be other metrics that can provide different or complementary information about the hypergraph. For instance, analysing the vertices present in the hyperedges can yield valuable insights. Moving forward, we plan to incorporate additional metrics that are based on different attributions of the hypergraph as spectrum of the hypergraph. These metrics will enhance our understanding of the hypergraph and provide a more comprehensive analysis of its properties.

## 4.1 Conclusion

In this work, we propose a new method for studying multidimensional datasets using filtration evolution of hypergraphs. The method allows for a comprehensive understanding of the data's properties, including its clustering behaviour and topological structure. The method was tested on different types of point distributions and dynamical systems, with different distance metrics found to be effective discriminators. The method was also applied to study the synchronization behaviour in the Kuramoto model and changes in brain network topology during seizures, demonstrating its potential for analysing complex multidimensional systems.

## Acknowledgements

This publication was supported by grand # MinCyT-FonCyT PICT-2019 N° 01750 PMO BID; grant CONICET-PUE-IMAL # 229 201801 00041 CO; grant CONICET-PIP-2021-2023-GI #11220200101940CO and grant UNL-CAI+D # 50620190100070LI

## References

- [1] C. Berge and C. Berge. Graphes et hypergraphes. 1970. *Dunod, Paris*, 1967.
- [2] C. Berge. Graphs and hypergraphs. 1973.
- [3] S. Zhang, Z. Ding, and S. Cui. Introducing hypergraph signal processing: Theoretical foundation and practical applications. *IEEE Internet of Things Journal*, 7(1):639–660, 2019.

- [4] S. Barbarossa and M. Tsitsvero. An introduction to hypergraph signal processing. In *2016 IEEE International Conference on Acoustics, Speech and Signal Processing (ICASSP)*, pages 6425–6429. IEEE, 2016.
- [5] O. N. Temkin, A. V. Zeigarnik, and D. G. Bonchev. *Chemical reaction networks: a graph-theoretical approach*. CRC Press, 2020.
- [6] E. V. Konstantinova and V. A. Skorobogatov. Application of hypergraph theory in chemistry. *Discrete Mathematics*, 235(1-3):365–383, 2001.
- [7] S. Feng, E. Heath, B. Jefferson, C. Joslyn, et al. Hypergraph models of biological networks to identify genes critical to pathogenic viral response. *BMC bioinformatics*, 22(1):1–21, 2021.
- [8] S. Klamt, U-U. Haus, and F. Theis. Hypergraphs and cellular networks. *PLoS computational biology*, 5(5):e1000385, 2009.
- [9] A. Dutta Choudhury and A. S. Chowdhury. Champs: Cardiac health hypergraph analysis using multimodal physiological signals. In *2019 41st Annual International Conference of the IEEE Engineering in Medicine and Biology Society (EMBC)*, pages 4640–4645. IEEE, 2019.
- [10] Y. Zhu, X. Zhu, M. Kim, J. Yan, D. Kaufer, and G. Wu. Dynamic hyper-graph inference framework for computer-assisted diagnosis of neurodegenerative diseases. *IEEE transactions on medical imaging*, 38(2):608–616, 2018.
- [11] J. Guo, H. Li, X. Sun, L. Qi, H. Qiao, Y. Pan, J. Xiang, and R. Ji. Detecting high frequency oscillations for stereoelectroencephalography in epilepsy via hypergraph learning. *IEEE Transactions on Neural Systems and Rehabilitation Engineering*, 29:587–596, 2021.
- [12] J. Yu, D. Tao, and M. Wang. Adaptive hypergraph learning and its application in image classification. *IEEE Transactions on Image Processing*, 21(7):3262–3272, 2012.
- [13] M. R. Gauthama Raman, N. Somu, K. Kirthivasan, R. Liscano, and V. S. Sriram. An efficient intrusion detection system based on hypergraph-genetic algorithm for parameter optimization and feature selection in support vector machine. *Knowledge-Based Systems*, 134:1–12, 2017.
- [14] X. Ouvrard. Hypergraphs: an introduction and review. *arXiv preprint arXiv:2002.05014*, 2020.
- [15] Y. Kuramoto. *Chemical turbulence*. Springer, 1984.
- [16] S. H. Strogatz. From kuramoto to crawford: exploring the onset of synchronization in populations of coupled oscillators. *Physica D: Nonlinear Phenomena*, 143(1-4):1–20, 2000.
- [17] J. A. Acebrón, L. L. Bonilla, C. J Vicente, F. Ritort, and R. Spigler. The kuramoto model: A simple paradigm for synchronization phenomena. *Reviews of modern physics*, 77(1):137, 2005.
- [18] F. A. Rodrigues, Thomas K. DM Peron, and J. Ji, P.and Kurths. The kuramoto model in complex networks. *Physics Reports*, 610:1–98, 2016.
- [19] J. L. Perez Velazquez, L. Garcia Dominguez, V. Nenadovic, and R. A. Wennberg. Experimental observation of increased fluctuations in an order parameter before epochs of extended brain synchronization. *Journal of biological physics*, 37:141–152, 2011.
- [20] C. J. Stam, G. Nolte, and A. Daffertshofer. Phase lag index: assessment of functional connectivity from multi channel eeg and meg with diminished bias from common sources. *Human brain mapping*, 28(11):1178–1193, 2007.

## A Basic Metrics

As we explained in Section 2, giving a set of points  $\chi$  we can use a metric to measure the distance between all pairwise components of the set, giving a  $n \times n$  distance matrix  $\mathcal{D}_\chi$ . In the sets considered in this paper, we used five different metrics that we proceed to define explicitly.

**Definition 2** Giving a set of point  $\chi \in \mathbb{R}^n$  with,  $\chi = \{\mathbf{x}_1, \dots, \mathbf{x}_m\}$  we define the component  $i, j = 1, \dots, m$  with  $j > i$  of the matrix distance  $\mathcal{D}_\chi$  as:

1. *Euclidean:*

$$\mathcal{D}_\chi^{Euc}(i, j) = \sqrt{\sum_{l=1}^n (\mathbf{x}_i^l - \mathbf{x}_j^l)^2}, \text{ where } \mathbf{x}_i = (x_i^1, \dots, x_i^n)$$

2. *Chebyshev:*

$$\mathcal{D}_\chi^{Cheb}(i, j) = \max_{l=1, \dots, n} |\mathbf{x}_i^l - \mathbf{x}_j^l|$$

3. *Cityblock:*

$$\mathcal{D}_\chi^{city}(i, j) = \sum_{l=1}^n |\mathbf{x}_i^l - \mathbf{x}_j^l|$$

4. *Minkowski:*

$$\mathcal{D}_X^{Mink}(i, j) = \left( \sum_{l=1}^n |x_i^l - x_j^l|^p \right)^{\frac{1}{p}}, \quad 1 \leq p < \infty$$

\* In this work we used  $p = 3$ .

5. *Parabolic:*

$$\mathcal{D}_X^{Par}(i, j) = \max_{l=1, \dots, n} |x_i^l - x_j^l|^{\alpha_l} \quad \text{with} \quad 0 < \alpha_l \leq 1, \quad l = 1, \dots, n.$$

\* In this work we used  $\alpha_1 = \alpha_2 = 1$  and  $\alpha_3 = 1/2$ .

## B Point Distribution Generation

### Normal distribution

A discrete random variable  $x$  is said to have a Normal distribution if:

$$p(x, \mu, \sigma^2) = \frac{1}{\sigma\sqrt{2\pi}} e^{-\frac{1}{2} \left( \frac{x - \mu}{\sigma} \right)^2}$$

where  $\mu$  is the location parameter, and it is going to be equal to the arithmetic mean and is the location parameter, and it is going to be equal to the arithmetic mean and  $\sigma^2$  is the standard deviation. In our work for the different realization, we use the function `random.normal` in numpy Python package.

### Poisson distribution

A discrete random variable  $x$  is said to have a Poisson distribution if:

$$p(x = k) = \lambda^k \cdot \frac{e^{-\lambda}}{k!}$$

Where  $k$  is an integer ( $k \geq 0$ ) and  $\lambda$  is a positive real number. The Poisson distribution describes the probability of encountering exactly  $k$  events in a time span if the events occur independently at a constant rate  $\lambda$ . To generate the distribution, we use the function `random.poisson` in numpy Python package.

### Uniform distribution

The uniform Distribution is given by the formula:

$$p(x, a, b) = \begin{cases} \frac{1}{b-a} & \text{for } a \leq x \leq b \\ 0 & \text{for } x < a \text{ or } x > b \end{cases}$$

In our work we use  $a = -1$  and  $b = 1$  and use the function `random.uniform` in numpy Python package.

### Lattice array

A lattice is an ordered array of points describing the arrangement of particles that form a crystal. In our work, we build the lattice defining a 3-dimensional cube and putting the data in a  $\mathbf{x}$ -distance position.

### Fractal array

For the fractal array, we generate  $N = 1000$  3D-points. The coordinates  $\mathbf{X} = [x^1, x^2, x^3]$  of each point followed the next pipeline. For each coordinate  $x^l$  we generate a vector of length  $L = 100$ ,  $\mathbf{x}^l = \{x_1^l, \dots, x_{100}^l\}$  with  $x_i^l$  randomly chosen between  $\{0, 3\}$  –for example  $\mathbf{x}^1 = \{0, 3, 0, 0, 0, 3, 0, \dots, 0\}$ –, then we measure the  $x^l$  values as.

$$x^l = \sum_{i=1}^L \frac{x_i^l}{4^i} \quad \text{for } l = 1, 2, 3$$

## C Dynamical System Generation

### Lorenz attractor

The Lorenz attractor is defined as the dynamical system governed by the following system of equations:

$$\begin{cases} \frac{dx}{dt} = \sigma(y - x) \\ \frac{dy}{dt} = -xz + rx - y \\ \frac{dz}{dt} = xy - bz \end{cases}$$

where we take the usual values  $\sigma = 10$ ,  $r = 284$ ,  $b = 8/3$  of the parameters. With the following initial conditions  $x_0 = 0$ ,  $y_0 = -0.01$  and  $z_0 = 9$

### Rössler attractor

The Rössler attractor is the attractor of the Rössler system, a system of three nonlinear ordinary differential equations

$$\begin{cases} \frac{dx}{dt} = -y - z \\ \frac{dy}{dt} = x + ay \\ \frac{dz}{dt} = b + z(x - c) \end{cases}$$

where we take the usual values of the parameters  $a = b = 0.2$ ,  $c = 5.7$ . With the following initial conditions  $x_0 = -9$ ,  $y_0 = 0$  and  $z_0 = 0$ .

### Complex butterfly attractor

The Complex butterfly attractor is a system of three nonlinear ordinary differential equations:

$$\begin{cases} \frac{dx}{dt} = a(y - z) \\ \frac{dy}{dt} = -z \operatorname{sgn}(x) \\ \frac{dz}{dt} = |x| - 1 \end{cases}$$

where we take the usual values of the parameters  $a = 0.55$ ,  $c = 5.7$ . With the following initial conditions  $x_0 = 0.2$ ,  $y_0 = 0$  and  $z_0 = 0$ .